General Disclaimer

One or more of the Following Statements may affect this Document

- This document has been reproduced from the best copy furnished by the organizational source. It is being released in the interest of making available as much information as possible.

- This document may contain data, which exceeds the sheet parameters. It was furnished in this condition by the organizational source and is the best copy available.

- This document may contain tone-on-tone or color graphs, charts and/or pictures, which have been reproduced in black and white.

- This document is paginated as submitted by the original source.

- Portions of this document are not fully legible due to the historical nature of some of the material. However, it is the best reproduction available from the original submission.

NGR - 33 - 008 - 146

A Numerical Method for Determination of Source Time Functions for General Three-Dimensional Rupture Propagation

Shamita Das

Lamont-Doherty Geological Observatory

of Columbia University

Palisades, New York 10964

Summary

We present a method to determine the displacement and the stress on the crack plane for a three-dimensional shear crack of arbitrary shape propagating in an infinite, homogeneous medium which is linearly elastic everywhere off the crack plane. The main idea of the method (which is due to Hamano) is to use a representation theorem in which the displacement at any given point on the crack plane is written as an integral of the traction over the whole crack plane. The tractions are weighted by the three-dimensional solution to Lamb's problem. Such solutions usually require one numerical integration, but fortunately the necessary solutions are obtainable in closed form. The weighting factor is discretized over a space and time grid to solve the integral equation numerically. As a test of the accuracy of our numerical technique, we compare the results with known solutions for two simple cases.

Introduction

It is now taken as a general working hypothesis that earthquakes (certainly shallow earthquakes) are produced by a sudden decrease of shear traction due to an instability which initiates at a point on some fault surface within the Earth. The rupture spreads over the fault surface and shearing motions develop further, behind the rupture front. The rupture stops at some later time either due to a strong barrier which it runs into or simply due to lack of strain energy, and the motion throughout the source region eventually ceases. Details in this broad picture need to be filled in, particularly with regard to the effects of spatially heterogeneous fault strength and initial stress. However, practical computations of displacements and stresses within faulting models of this type having any fault shape have not yet been done even for a planar fault surface lying in an unbounded, isotropic elastic medium.

For certain special geometries of faulting, a great deal is known. The most widely studied involve rupture fronts which initiate and move as an infinite line. [From an enormous literature, one may cite the key papers of Kostrov (1966), Burridge (1969), Freund (1976), Andrews (1976) and Das & Aki (1977a,b).] From these two-dimensional studies, a quantitative picture has begun to emerge of how the distribution of fault strength will affect rupture propagation. Important though this is, such models are inherently limited in their ability to explain gross features of faulting because many aspects of the earthquake source demand a three-

dimensional analysis. For instance, motions at an earthquake source initiate in a highly localized region (a point, rather than along an infinite line), and plane strain and antiplane strain are present simultaneously (possibly being coupled together) around the general rupture front. The special geometry of elliptical (including circular) cracks has been assumed by many authors to model earthquake faults (e.g., Kostrov 1964; Burridge & Willis 1969; Richards 1976; Madariaga 1976). Here again, this special assumption has led to some progress, both for near-field studies, and for the study of stopping phases. The major limitation of published methods is that the areal growth of faulting has had to be specified, rather than itself becoming a part of the solution for spontaneous crack growth. Thus, even for a crack which starts out with an elliptical shape, there has been no investigation to see if this shape will be maintained coherently during crack growth. Mikumo & Miyatake (1978) have suggested that major irregularities in slip can develop during dynamic faulting. They use a finite difference method for solving for the elastic motions, and their results are qualitatively appealing. However, it should be pointed out that due to inadequate computer storage, these authors had to place a rigid spatial boundary parallel to the fault surface, at only one grid spacing from the fault. Reflections from such a surface clearly modify the computed fault slip and prevent an accurate account of the effects of radiation of elastic waves away from the source region.

In this paper, we present a numerical method which is an extension of Hamano's (1974) numerical method for two-dimensional problems [described in detail by Das & Aki (1977a)]. The method is capable of handling three-dimensional spontaneous rupture propagation with variable fault strength and variable stress drop. In this paper, we shall not study these general problems but only present the details of the method and show that the method works by comparison with available analytical and numerical solutions for two very simple cases. The application of the method to actual faulting processes will be discussed in a future paper.

Table of symbols (in alphabetical order)

F = discretized values of g at the origin

$F(x_{1i},x_{2j},0,t_k)$ = discretized value of g at $(x_{1i},x_{2j},0,t_k)$

$g_{ni}(\underset{\sim}{x},t;\underset{\sim}{y},s)$ = three-dimensional Green's function for a homogeneous half-space.

$g_{ni}^{H}(\underset{\sim}{x},t;\underset{\sim}{y},s)$ = response of three-dimensional homogeneous, half-space for a unit step source time function

r,ϕ = polar coordinates on crack plane $x_3 = 0$.

S_1 = crack region on crack plane $x_3 = 0$

S_2 = region outside crack on plane of crack

t,s = time

Δt = grid-spacing in time

T	$= \alpha t/r$
$u_i(\underset{\sim}{x},t)$	= displacement component in x_i-direction
x_1, x_2, x_3	= cartesian coordinates
Δx	= grid spacing in x_1 and x_2 directions.
α	= compressional wave speed
β	= shear-wave speed
γ	= Rayleigh wave speed
σ_d	= dynamic frictional stress.
σ_{ij}, τ_{ij}	= stress components acting on crack plane $x_3 = 0$
τ_e	= effective stress or "dynamic stress drop".

Formulation of problem

We model the earthquake source as a propagating plane shear crack in an infinite homogeneous, elastic solid, radiating energy out into three spatial dimensions. The geometry of the crack is shown in Fig. 1. Let $x_3 = 0$ be the plane across which slip occurs. Initially, the infinite body is under a uniform state of stress σ_{ij}°. The stress on the fault plane $x_3 = 0$ can be separated into the normal stress σ_{33}° and a shear stress $\sigma_{13}^\circ = \sigma^\circ$, say. The component σ_{23}° can be taken to be zero by taking the axis x_1 in the direction of maximum initial shear.

Let us assume that the initial shear stress is increased so that the crack extends along the plane $x_3 = 0$. The normal stress σ_{33}° over the plane $x_3 = 0$ remains constant throughout the rupture process (Richards 1976). Let us take the origin of time $t = 0$ as the time when the crack starts extending. The extension of the crack may be rapid enough to generate elastic

waves. The tip of the crack may move at some predetermined velocity or the position of the crack tip as a function of time may be found using the state of stress near the crack tip and an appropriate fracture criterion. In this paper we shall only consider the former case. As the crack extends, there is relative motion between the regions $x_3 < 0$ and $x_3 > 0$ and a displacement discontinuity occurs across the $x_3 = 0$ plane. This discontinuity in displacement is a function only of the coordinate x_1, x_2, and time t. The shear stress on the crack surface is zero if there is complete stress release or is equal to the dynamic frictional stress σ_d given by $\mu_d \sigma_{33}^{\circ}$ on the crack surface. μ_d is the dynamic coefficient of friction (which can be taken as a constant or a function of space and time). Let the incremental stresses due to the displacements $\vec{u}$ from initial configuration be τ_{ij}, so that $\sigma_{ij} = \sigma_{ij}^{\circ} + \tau_{ij}$ i.e., τ_{ij} is the stress change due to the motion. We shall solve the problem for τ_{ij}. (An initially nonhomogeneous state of stress can be incorporated into the method.)

We shall assume that the initial conditions are that the displacements and velocities are zero everywhere in the medium. We discuss next the symmetry of the displacements and stresses across the plane $x_3 = 0$.

Das (1976) showed that the quantities τ_{23}, τ_{13} and u_3 are even across the plane $x_3 = 0$ and τ_{33}, u_1 and u_2 are odd across the plane $x_3 = 0$, by considering the equations of motion satisfied by the u_i's and the fact that τ_{13}, τ_{23}, τ_{33}, and u_3 are continuous across the crack plane $x_3 = 0$ and u_1 and u_2 are continuous across the portion of $x_3 = 0$ outside the crack

but discontinuous across the portion of $x_3 = 0$ containing the crack. For the cracked region of the plane $x_3 = 0$, we can therefore write

$$u_1 (x_1, x_2, +0, t) = -u_1 (x_1, x_2, -0, t) = (1/2)\Delta u_1$$
$$\text{and } u_2 (x_1, x_2, +0, t) = -u_2 (x_1, x_2, -0, t) = (1/2)\Delta u_2$$

where Δu_1 and Δu_2 are, respectively, the relative displacements in the x_1 and x_2 directions across the $x_3 = 0$ plane. For the unbroken region of $x_3 = 0$, $u_1 = 0$, $u_2 = 0$. Thus there is a symmetry in the problem about the plane $x_3 = 0$. Owing to this symmetry, it will be sufficient to solve the problem in a half-space bounded by the plane containing the crack, i.e., the $x_3 = 0$ plane.

Let us divide the crack plane $x_3 = 0$ into the crack region S_1 and the region outside the crack S_2. (The normal stress τ_{33} across the fault is zero everywhere on $x_3 = 0$ since τ_{33} is odd and continuous across $x_3 = 0$.) In S_1, we therefore have:

τ_{13}, τ_{23} are known; $\tau_{33} = 0$; u_1, u_2, u_3 unknown.

In S_2, τ_{13}, τ_{23} are unknown; $\tau_{33} = 0$; $u_1 = 0$, $u_2 = 0$ and $u_3 \neq 0$ is unknown.

Using the relation $\sigma_{ij} = \sigma_{ij}^{\circ} + \tau_{ij}$, the boundary conditions finally are:

In S_1: $\tau_{23} = 0$, $\tau_{13} = -\tau_e = (\sigma_d - \sigma^{\circ})$ where τ_e is called the "dynamic stress drop" or the "effective stress".
$\tau_{33} = 0$
u_1, u_2, u_3 are unknown.

In S_2: $u_1 = 0$, $u_2 = 0$, $\tau_{33} = 0$, $u_3 \neq 0$ (unknown) (1)
τ_{13}, τ_{22} unknown.

This gives a mixed boundary value problem for a very general three-dimensional rupture propagation problem including mixed-mode ruptures.

The integral equation for the three components of displacement can, in general, be written as [pg. 29 of Das (1976), also Aki & Richards (1980) eq. 2.43]

$$u_n(\underset{\sim}{x},t) = \int_{-\infty}^{\infty} ds \int_{S'} n_j \, G_{ni}^{free}(\underset{\sim}{x},t;\underset{\sim}{y},s)\tau_{ij}(\underset{\sim}{y},s)dS'(\underset{\sim}{y})$$

where the Green function $G_{ni}^{free}(\underset{\sim}{x},t;\underset{\sim}{y},s)$ is the displacement in the n-direction at the point $(x_1,x_2,0)$ at time t at the free surface due to a unit impulse acting in the i-direction at $(y_1,y_2,0)$ at time s at the free surface, and S' is the bounding surface of the elastic half-space (i.e., the infinite plane containing the crack). Since $x_3 = 0$, $y_3 = 0$ in our case, the dependence on $\underset{\sim}{y},\underset{\sim}{x},s,t$ is only via (y_1-x_1), (y_2-x_2), 0,0 and (t-s), and so $G_{ni}^{free}(\underset{\sim}{x},t;\underset{\sim}{y},s) = g_{ni}(y_1-x_1,y_2-x_2,0,0,t-s)$. On the fault plane $x_3 = 0$ we get

$$\begin{aligned}
u_1(x_1,x_2,0,t) = \int_{-\infty}^{\infty} ds \iint_{-\infty}^{\infty} & [g_{11}(y_1-x_1,y_2-x_2,0,0,t-s)\tau_{13}(y_1,y_2,0,s) \\
& + g_{12}(y_1-x_1,y_2-x_2,0,0,t-s)\tau_{23}(y_1,y_2,0,s) \\
& + g_{13}(y_1-x_1,y_2-x_2,0,0,t-s)\tau_{33}(y_1,y_2,0,s)]dy_1dy_2 \\
u_2(x_1,x_2,0,t) = \int_{-\infty}^{\infty} ds \iint_{-\infty}^{\infty} & [g_{21}(y_1-x_1,y_2-x_2,0,0,t-s)\tau_{13}(y_1,y_2,0,s) \\
& + g_{22}(y_1-x_1,y_2-x_2,0,0,t-s)\tau_{23}(y_1,y_2,0,s) \\
& + g_{23}(y_1-x_1,y_2-x_2,0,0,t-s)\tau_{33}(y_1,y_2,0,s)]dy_1dy_2 \qquad (2) \\
u_3(x_1,x_2,0,t) = \int_{-\infty}^{\infty} ds \iint_{-\infty}^{\infty} & [g_{31}(y_1-x_1,y_2-x_2,0,0,t-s)\tau_{13}(y_1,y_2,0,s) \\
& + g_{32}(y_1-x_1,y_2-x_2,0,0,t-s)\tau_{23}(y_1,y_2,0,s) \\
& + g_{33}(y_1-x_1,y_2-x_2,0,0,t-s)\tau_{33}(y_1,y_2,0,s)]dy_1dy_2
\end{aligned}$$

[The terms g_{13}, g_{23} and g_{33} are included to study tension cracks.]

The region of integration for the system of integral equations is defined by the causality condition. Taking the P-wave velocity $\alpha = 1$, the equation for the region over which Green's function is non-zero is

$$(t-s) - \sqrt{(y_1-x_1)^2 + (y_2-x_2)^2 + y_3^2} \geq 0, \quad t \geq s \geq 0.$$

For $x_3 = 0$, this reduces to the cone S (Fig. 2) defined by

$$(t-s)^2 - (y_1-x_1)^2 - (y_2-x_2)^2 \geq 0, \quad t \geq s \geq 0. \tag{3}$$

Thus the integrations in the integral equations extend over this conical region only. To find the displacements inside the crack, it is necessary to solve the system of three integral equations under the initial and boundary conditions discussed above. (It is not necessary to determine the displacement component u_3, which gives the displacement normal to the crack plane, as long as we are interested in looking only at the slip on the fault plane.) The region of integration includes the region S_2 outside the crack (but within the backward characteristic cones) where the stress components τ_{12} and τ_{23} are unknown. So we must first determine these stresses. This can be done as long as the crack-tip velocity is known - either assumed a priori or determined by use of some fracture criterion, as we shall show in a later section.

4. Green's function for the three-dimensional problem

To solve for u_1 and u_2 in the system of equations (2), we need Green's functions g_{11}, g_{12} $(= g_{21})$ and g_{22}, where, for example, by g_{12} we mean that

$$g_{12}(x_1,x_2,0,t;0,0,0,s)$$

is the displacement in the x_1-direction, at position $(x_1,x_2,0)$ and time t, due to a unit impulse applied in the x_2-direction at the origin at time s. Richards (1979) has analytically solved Lamb's problem and obtained closed form solutions for the case when the applied force is a unit step in time rather than an impulse. Let us call these Green's functions g_{11}^H, g_{12}^H and g_{22}^H. Then we simply need to find the time-derivative of these quantities to obtain the Green's functions we require for our problem, so that $g_{11} = \frac{d}{dt} g_{11}^H$, etc.

The four Green's functions are given in terms of two dimensionless functions $I_1(T)$ and $I_2(T)$ via

$$\begin{aligned} g^H_{11} &= [I_1(T)\cos^2\phi - I_2(T)\sin^2\phi]/(\pi\mu r) \\ g^H_{12} &= g^H_{21} = [I_1(T)+I_2(T)]\cos\phi\sin\phi/(\pi\mu r) \\ g^H_{22} &= [I_1(T)\sin^2\phi - I_2(T)\cos^2\phi]/(\pi\mu r). \end{aligned} \tag{4}$$

where,

$$x_1 = r\cos\phi, \quad x_2 = r\sin\phi, \quad T = \alpha t/r. \tag{5}$$

and

$$I_1(T) = \begin{cases} 0 & \text{for } T < 1, \\ T^2\{c_1/(T^2-T_1^2)^{\frac{1}{2}} + c_2/(T^2-T_2^2)^{\frac{1}{2}} - c_3/(T_3^2-T^2)^{\frac{1}{2}}\} & \text{for } 1 < T < (\alpha/\beta), \\ 0.5 - 2T^2c_3/(T_3^2-T^2)^{\frac{1}{2}} & \text{for } (\alpha/\beta) < T < T_3 \equiv (\alpha/c_R), \\ 0.5 & \text{for } T_3 < T. \end{cases} \tag{6a}$$

$$I_2(T) = \begin{cases} 0 & \text{for } T < 1, \\ -c_4+c_1(T^2-T_1^2)^{\frac{1}{2}}+c_2(T^2-T_2^2)^{\frac{1}{2}}+c_3(T_3^2-T^2)^{\frac{1}{2}} & \text{for } 1 < T < (\alpha/\beta), \\ -2c_4+2c_3(T_3^2-T^2)^{\frac{1}{2}} & \text{for } (\alpha/\beta) < T < T_3, \\ -2c_4 & \text{for } T_3 < T. \end{cases} \tag{6b}$$

The constants T_1^2, T_2^2, T_3^2 are solutions to the Rayleigh cubic equation, and in fact $T_3 = \alpha/c_R$ where c_R is the Rayleigh wave speed. c_1, c_2, c_3 and c_4 are positive constants, for a homogeneous elastic medium of given Poisson's ratio less than 0.263. The seven constants $T_1^2, \ldots, c_4$ need be evaluated just once for a given elastic medium, and then the computation of our Green's functions reduce to taking at most three square roots, and performing on the order of ten multiplications and divisions.

Fig. 3 shows the quantities I_1 and I_2 as found by Richards (1979) for the case $\alpha = \sqrt{3}\beta$, and the time-derivatives of I_1 and I_2, for the same case. Note the singularities in I_1 and I_2 and in $\partial I_1/\partial t$ and $\partial I_2/\partial t$. Note also that for the three-dimensional Green's function with an impulsive source, the displacements become zero once the Rayleigh wave has passed. This results in a drastic reduction in the computer storage necessary to store the g's, unlike the two-dimensional problem where the disturbance never ceases. Note also that g_{11} and g_{22} are simply 90° rotations of one another so we only have to determine g_{11} and g_{12}. Also g_{11} itself is symmetric about the x_1 and x_2 axes so we only have to calculate it in one quadrant. g_{12} has an eight-fold symmetry and needs to be calculated only in half of one quadrant.

5. Numerical method of solving the system of integral equations

The integral equations (2) are of the general form

$$u(x_1,x_2,0,t) = \iiint g(x_1-y_1,x_2-y_2,0,0,t-s)\tau(y_1,y_2,0,s)dy_1dy_2ds \quad (7)$$
$$+ \ldots + \ldots$$

In order to solve (7) numerically, we divide the (x_1,x_2,t) volume into elements, each having length Δx along the x_1 and x_2 direction and Δt along the t-direction. The grid points are the centres of these elements and are given by $x_1 = \ell\Delta x$, $x_2 = m\Delta x$, $t = n\Delta t$, where $\ell,m = 0,\pm1,\pm2, \ldots$, $n = 0,1,2, \ldots$ The stresses are assumed to be constant within each element. The kernel g has to be discretized so that the integrals in (7) can be replaced by summation over grids. We discretize g by averaging g over each volume element. Then the discretized g is

$$F(x_{1i},x_{2j},0,t_k) = \frac{1}{\Delta x\Delta x\Delta t} \int_{t_k-\Delta t/2}^{t_k+\Delta t/2} dt \int_{x_{1i}-\Delta x/2}^{x_{1i}+\Delta x/2} dx_1 \int_{x_{2j}-\Delta x/2}^{x_{2j}+\Delta x/2} g(x_1,x_2,0,0,t)dx_2$$

where $x_{1i}^2+x_{2j}^2 \leq \alpha^2t^2_k$, α = P-wave velocity

Interchanging orders of integration (which is allowable as long as the limits of the integration over x_1 and x_2 are not functions of time), we get

$$= \frac{1}{\Delta x \Delta x \Delta t} \int_{x_{1i}-\Delta x/2}^{x_{1i}+\Delta x/2} dx_1 \int_{x_{2j}-\Delta x/2}^{x_{2j}+\Delta x/2} dx_2 \; [g^H(x_1,x_2,0,0,t_k+\Delta t/2)-g^H(x_1,x_2,0,0,t_k-\Delta t/2)]$$

Transforming to r,ϕ coordinates (by equation (5)), we find that we are able to do the integration over r analytically. The integration over ϕ has to be done numerically. Due to the symmetries (or antisymmetries) in the g's as discussed before, we only have to do the numerical integration over one quadrant for the g_{11}'s and over half of one quadrant for the g_{12}'s. For the points lying along the t-axis (including the origin of the (x_1,x_2,t) coordinate system, we were able to do the integrations over both r and ϕ analytically. Note that the 1/r type singularity in the Green functions (equation (4)) does not cause any problem even at r = 0 since 1/r can be integrated over an area about the origin to give a finite value (c.f., Andrews 1974).

Discretizing the integral equation (7), we obtain the matrix equation

$$u(x_{1i},x_{2j},0,t_k) = \Delta x \Delta x \Delta t \sum_{l,m,n} [F(x_{1i}-x_{1l},x_{2j}-x_{2m},0,0,t_k-t_n)\tau(x_{1l},x_{2m},0,t_n) + \ldots + \ldots] \quad (8)$$

where $(x_{1i},x_{2j},0,t_k)$ refers to the observation point. It should be pointed out that in equation (8) one can use variable values of Δx and Δt in the region of integration. In other words, the cone of integration S can be divided into finer grids at some places than others, e.g., if one is interested in studying more closely the behaviour at the crack-tip, one can divide the region near the crack-tip into finer grids than regions farther away from the crack tip. This is useful in determining, say, the amount

of energy absorbed at the crack-tip during the rupture process. In this respect, the integral equation technique is analogous to finite-element methods which allow variable grid-sizes. However, implementation of this variable grid-size is not a trivial problem and for now we shall consider only constant grid-sizes.

Figure 4 shows a plot of the discretized g_{11} at a certain instant in time. Note that as expected, there is no P-wave along the x_2-axis.

To determine the stresses τ_{13} and τ_{23} in S_2, we make use of the boundary conditions that $u_1 = 0$ and $u_2 = 0$ in S_2. Then, from the integral equations, we get

$$0 = \int dt \iint [g_{12}(..)\tau_{23}(\ ) + g_{11}(..)\tau_{13}(\ )]dy_1dy_2$$

$$0 = \int dt \iint [g_{22}(\ )\tau_{23}(\ ) + g_{21}(\ )\tau_{13}(\ )]dy_1dy_2.$$

The region of integration is the same backward characteristic cone S defined in (3). Writing the two above equations in the discrete form and taking the term for which $x_1 = y_1$, $x_2 = y_2$ and $s = t$ to the L.H.S., we get

$$F_{12}\tau_{23}(x_1,x_2,0,t) + F_{11}\tau_{13}(x_1,x_2,0,t)$$
$$= \quad - \Sigma\Sigma\Sigma \quad [g_{12}(..)\tau_{23}(..)+g_{11}(...)\tau_{13}(...)]$$
$$\text{sum over}$$
$$x_1,x_2,s$$
$$= L, \text{ say}$$

$$F_{22}\tau_{23}(x_1,x_2,0,t) + F_{21}\tau_{13}(x_1,x_2,0,t)$$

$$= \underset{\text{sum over } x_1,x_2,s}{-\Sigma\Sigma\Sigma} [g_{22}(..)\tau_{23}(..)+g_{21}(..)\tau_{13}(...)]$$

$$= M, \text{ say}$$

where F_{ij} are the known values of the Green function g_{ij} averaged over the grid centered at the origin of the coordinate system. The summation extends over every point of the cone S except the vertex. Due to the symmetries in the Green functions, it follows that:

$$F_{ij} = 0, \text{ if } i \neq j$$

$$\neq 0, \text{ if } i = j.$$

Also, $F_{11} = F_{22}$. Hence, the unknown stresses are determined as

$$\tau_{13}(x_1, x_2, 0, t) = \frac{L}{F_{11}}$$

and $$\tau_{23}(x_1, x_2, 0, t) = \frac{M}{F_{11}}$$

6. Instantaneous circular shear crack

We study the case of an instantaneous circular fault of finite radius that suddenly appears and starts radiating without growing. This is a non-physical problem as it violates causality. We study it simply to check the accuracy of our numerical technique by comparing it with the results of Madariaga (1976) who studied the same problem using a completely different numerical technique viz. a finite difference technique. Our results are shown in Fig. 5. The radius of the circular fault was $4.5\Delta x$ and we took $\alpha\Delta t/\Delta x = .5$. The slip at a point inside the crack was stopped when the slip velocity at the point tended to reverse sign. We show results for various radial distances along the crack. Note that we plot total slip so that the results of equation (8) need to be doubled. The normalization factor for the slip is $a\tau_e/\mu$, where a is the fault radius, τ_e is the dynamic stress-drop, μ is the rigidity. The points where the P stopping phases from the nearest and farthest edge of the fault arrive at a given point is shown by crosses and open circles, respectively. The point at which the fault healed is indicated by closed circles. Comparison with Fig. 2 of Madariaga (1976) shows that in general our results compare well with his. It is found that the fault generally starts healing about the time when the P-stopping phase from the farthest edge arrives. Madariaga found that every point of the fault healed almost simultaneously. The final slip after the fault has healed was found by Madariaga to be $u_1 = \frac{\tau_e a}{\mu}$ (1.52) at the centre of the crack. The static solution for this case is $u_1 = \frac{12}{7\pi}\frac{a\tau_e}{\mu}\sqrt{1-r^2/a^2}$, where r = distance from the centre of the fault. Madariaga's solution thus overshoots the static solution at

the centre by a factor of 1.34. We find that our final slip at the centre is virtually the same as Madariaga's. The slip at points $\frac{r}{a} = .22$ (not plotted), $\frac{r}{a} = .44$, $\frac{r}{a} = .66$ and $\frac{r}{a} = .88$ overshoot the static solution at these points by factors of 1.31, 1.25, 1.2 and 1.0, respectively, in our case. Madariaga found that the slip at the points r/a = .2, .4, .6 and .8 overshoots the static solution at these points by factors of 1.25, 1.18, 1.22 and 1.21, approximately. This implies that the centre of the fault overshoots the static solution more than the edges and that the final static stress drop is not a constant over the whole fault but is greater at the centre of the fault than near the edges. This non-uniform stress drop is a consequence of our healing specification.

We also point out here that for a circular crack there is an azimuthal symmetry in displacement, stress, and velocity fields. We have <u>not</u> assumed such a symmetry but have calculated the fields in one whole quadrant of the circular fault. The results have the required azimuthal symmetry. That is, in every direction from the centre of the fault the displacements and stresses are the same within 15% (in the worst case).

7. Circular crack which grows at speed $\alpha/2$

We next study the case of a circular crack that starts from a radius of $1.5\Delta x$ and grows at half the P-wave speed. In Fig. 6 we show numerical results for two cases: one for a self-similar circular crack that never stops and the other for a circular crack that stops when it reaches a radius of $6.5\Delta x$. The latter solution is shown by dotted lines, where it diverges from the former solution.

a. Self-similar crack

The half-slip, plotted at various radial distances along the fault, is normalized by the factor $(\frac{\Delta x\ \tau_e}{3\mu})$. The analytical solution for the half-slip for a circular self-similar shear crack which initiates at a point and grows at a speed of $\alpha/2$ can be determined from Kostrov (1964) or Dahlen (1974) to be $u_1 = .69\sqrt{t^2-4r^2}$, using the same normalization factor as we have used, where r is the radius at time t.

The analytical solution is shown on the figure as continuous lines. For the case when the crack stops, the arrival of the P-stopping phase from the nearest crack edge is indicated. The slip is stopped when the slip velocity tends to reverse sign. Our numerical solution compares well with the analytic solution. The solution for the points closer to the centre are initially larger than the analytic solution but converge to the analytic solution at later times. For points farther away from the centre, this effect is not seen. This is due to the fact that in the analytic solution the rupture initiated at a point, whereas in our problem the initial rupture area is finite. The displacement at a point immediately after it breaks shows the sharp rise as is expected from the analytic solution. This is in contrast to the results of Madariaga (1976) who uses numerical damping to smooth the stresses and velocities at the crack tip and thereby loses the detailed behaviour at the crack-tip.

We plot in Fig. 7 the slip velocities determined by numerical differentiation using the relation $\dot{u}_1(t) = \frac{u_1(t+\Delta t)-u_1(t-\Delta t)}{2\Delta t}$ at various radial distances and azimuths from the centre of the fault. The numerical differentiation introduces high-frequency noise into our results. The numerical solution oscillates about the analytic solution and does not diverge significantly from it. This is a very important property of our result

since pulse shapes due to a rupture depend on the slip velocities on the rupture surface. In fact, since the determination of pulse-shapes involves integration of these slip-velocities over the fault surface, these oscillations will be drastically reduced and will not affect the pulse-shapes.

Fig. 7 also shows that our results have azimuthal symmetry about the origin, even though such a symmetry was not assumed. In our problem, we took the x_1-direction to be along the direction of the initially applied shear stress. For a self-similar crack, this means that the component of displacement u_2 and the component τ_{23} of the shear stress on the crack surface are both zero. We calculate both these quantities to check if they are zero. We find that u_2 and τ_{23} are both very small. The reason for u_2 and τ_{23} not being exactly zero is numerical noise due to the discrete nature of the problem. In fact, u_2 and τ_{23} may be taken as a rough measure of the numerical noise in the u_1 and τ_{13} components, respectively.

We find that u_2 is never larger than 8% of u_1 and does not increase with time. τ_{23} is found to be always less than 20% of the dynamic stress drop. Both u_2 and τ_{23} show azimuthal symmetry about the centre of the crack.

Thus we find that even though our grid-spacing is fairly rough, so that we have only a crude approximation to a circular crack which extends discontinuously and we have slightly different initial conditions than that necessary for a self-similar crack, our results compare well with the analytic solution. The only restriction is that we are limited in the upper limit of frequencies of radiation we can study with this technique.

b. Finite crack

The results for a circular crack that starts from a radius of $1.5\Delta x$, grows at $\alpha/2$ and is stopped when it reaches a final radius of $6.5\Delta x$ is shown in Fig. 6 by dotted lines where it deviates from the self-similar solution. The normalization factor for the half-slip is $(a\tau_e/3\mu)$. The final offset at any point on the crack is given by

$$u_1 = (1.23)\,\frac{12}{7\pi}\,\frac{\tau_e}{\mu}\,\sqrt{a^2 - r^2}\quad ,$$

so that the dynamic solution overshoots the static solution by 23%. For the same problem using different numerical techniques, Madariaga (1976) found an overshoot of 20% and Archuleta (1976) an overshoot of 27%.

Conclusions

We have developed a numerical scheme based on a boundary-integral equation technique to determine the slip on the fault surface for a three-dimensional shear crack of any arbitrary shape. We have shown by comparison with available solutions for simple cases that the technique works correctly. The advantage of this method is that it can incorporate a fracture criterion so as to enable the study of spontaneous crack propagation. Further, it can be used to study the case when there is variable strength, variable initial stress, and variable friction on the crack surface. Study of these cases is now underway. The computing time for fifty time-steps for $\alpha\Delta t/\Delta x = .5$ was 15 minutes of CPU time on an IBM 360/75 or IBM 360/91. The method can also be applied to study the propagation of tension cracks by using the appropriate components of Green's functions, which are available from Richards (1979).

Acknowledgements

I would like to thank Paul Richards and Chris Scholz for critically reviewing the manuscript and for discussions and encouragement throughout the course of this work. Extensive discussions with Jack Boatwright are also gratefully acknowledged. The author would also like to thank Lamont-Doherty Geological Observatory for a Lamont-Doherty Postdoctoral Fellowship during the course of this work. Partial support was provided by National Science Foundation grant EAR 79-01810 and by the National Aeronautics and Space Administration grant NGR 33-008-146.

References

Aki, K. & Richards, P.G., 1980. Quantitative Seismology: Theory and Methods, ∿ 1800 p., W.H. Freeman and Company, San Francisco, California, 1980, in press.

Andrews, D.J., 1974. Evaluation of static stress on a fault plane from a Green's function, Bull. Seismol. Soc. Am., 64, 1629-1633.

Andrews, D.J., 1976. Rupture velocity of plane strain shear cracks, J. Geophys. Res., 81, 5679-5687.

Archuleta, R.J., 1976. Experimental and numerical three-dimensional simulations of strike-slip earthquakes, Ph.D. Dissertation, Univ. California, San Diego.

Burridge, R., 1969. The numerical solution of certain integral equations with non-integrable kernels arising in the theory of crack propagation and elastic wave diffraction, Phil. Trans. Roy. Soc. Lond., A265, 353-381.

Burridge, R. & Willis, J.R., 1969. The self-similar problem of the expanding elliptical crack in an anisotropic solid, Proc. Camb. Phil. Soc., 66, 443-468, 1969.

Dahlen, F.A., 1974. On the ratio of P-wave to S-wave corner frequencies for shallow earthquake sources, Bull. Seismol. Soc. Am., 64, 1159-1180.

Das, S., 1976. A numerical study of rupture propagation and earthquake source mechanism, Sc.D. Thesis, Massachusetts Institute of Technology, Cambridge, Massachusetts.

Das, S. & Aki, K., 1977a. A numerical study of two-dimensional spontaneous rupture propagation, Geophys. J. R. astr. Soc., 50, 643-668.

Das, S. & Aki, K., 1977b. Fault plane with barriers: a versatile earthquake model, J. Geophys. Res., 82, 36, 5658.

Freund, L. B., 1976. Dynamic crack propagation, in The Mechanics of Fracture, AMD, 19, edited by F. Erdogan, ASME, 105-134.

Hamano, Y., 1974. Dependence of rupture time history on the heterogeneous distribution of stress and strength on the fault plane (abstract), EOS, Trans. Am. Geophys. Un., 55, 352.

Kostrov, B.V., 1964. Selfsimilar problems of propagation of shear cracks, J. Appl. Math. Mech., 28, 1077-1087.

Kostrov, B.V., 1966. Unsteady propagation of longitudinal shear cracks, J. Appl. Math. Mech., 30, 1241-1248.

Madariaga, R., 1976. Dynamics of an expanding circular fault, Bull. Seismol. Soc. Am., 66, 639-666.

Mikumo, T. & Miyatake, T., 1978. Dynamical rupture process on a three-dimensional fault with nonuniform frictions and near-field seismic waves, Geophys. J. R. astr. Soc., 54, 417-438.

Richards, P.G., 1976. Dynamic motions near an earthquake fault: a three-dimensional solution, Bull. Seismol. Soc. Am., 66, 1-32.

Richards, P.G., 1979. Elementary solutions to Lamb's problem for a point source and their relevance to three-dimensional studies of spontaneous crack propagation, Bull. Seismol. Soc. Am., 69, 947-956.

Figure Captions

Figure 1. Schematic representation of fault geometry. x_1 is the direction of initial applied stress and $x_3 = 0$ is the fault plane.

Figure 2. Region of integration in (x_1, x_2, t) space. Shaded region in lower figure is the cone S defined in equation (3). In the upper figure, the cone S is projected on the $x_2 = 0$ plane for clarity.

Figure 3. Figure showing time-dependence of I_1, I_2, $\frac{\partial I_1}{\partial t}$ and $\frac{\partial I_2}{\partial t}$ for the case $\alpha^2 = 3\beta^2$. The dotted lines are the values of the function increased ten-fold to show detailed behaviour at low amplitudes. P, S and R are the arrival times of the compressional, shear and Rayleigh waves. Values are plotted as heavy lines only between amplitudes ±1 for I_1 and I_2 and amplitudes ± 10 for $\frac{\partial I_1}{\partial t}$, $\frac{\partial I_2}{\partial t}$. In fact, I_1 is singular at R, $\frac{\partial I_1}{\partial t}$ is singular at P and R and $\frac{\partial I_1}{\partial t}$ is singular at S and R.

Figure 4. Three-dimensional plot of the discretized Green's function component $F_{11}(x_1, x_2, t)$ at $t = 17.5\Delta x / \alpha$. 1 and 2 are the directions x_1 and x_2. 0 is the point of application of impulse. P, S and R indicate the compressional, shear and Rayleigh waves.

Figure 5. Normalized slip function for an instantaneously appearing circular fault. The normalization factor for the time is $\frac{\alpha t}{a}$ and for the slip is $\frac{3\mu}{a\tau_e}$, where τ_e is the stress drop, μ is the rigidity, and a is the fault radius. The slip is shown at several radial distances from the origin. The P-wave speed was taken as unity. The static solution at the centre of the crack is at the level 1.1. The crosses and open circles indicate arrival of the P-stopping phase from the nearest and farthest edges of the fault. The solid circles indicate the time when the point healed.

Figure 6. Normalized half-slip for a circular self-similar shear crack which grows at speed $\alpha/2$. The continuous lines are the analytic solution due to Kostrov (1964). The step-like solid lines give the numerical solution. The step-like dotted lines are the solution for the case when the crack stops suddenly after reaching a radius of $6.5\Delta x$

Figure 7. Normalized slip velocities for a circular self-similar shear crack which grows at a speed of $\alpha/2$. The continuous lines are the analytic solution given by $\dot{u}_1 = .69t/\sqrt{t^2-4r^2}$. The numerical solutions are shown by crosses and solid circles.

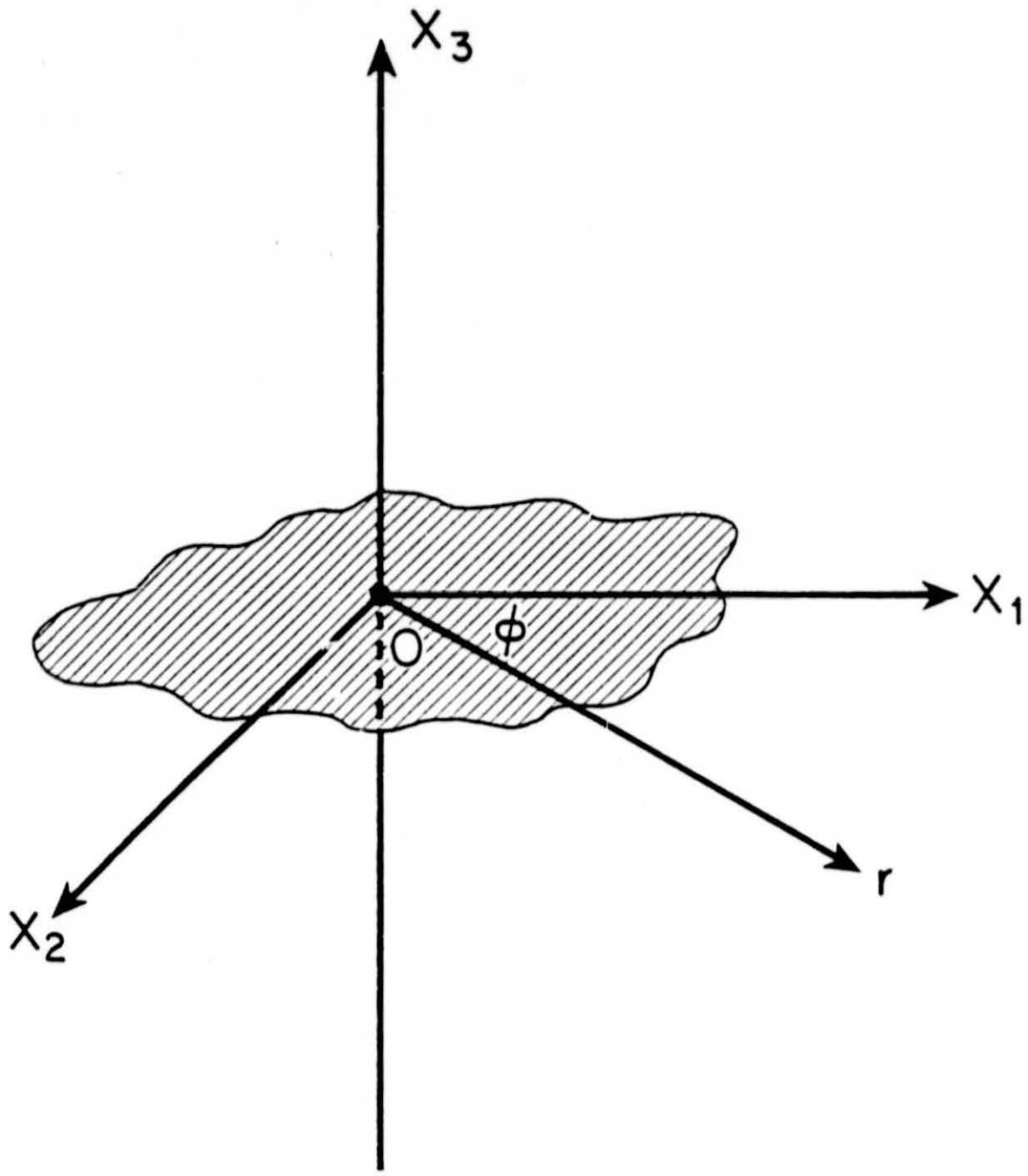

Figure 1

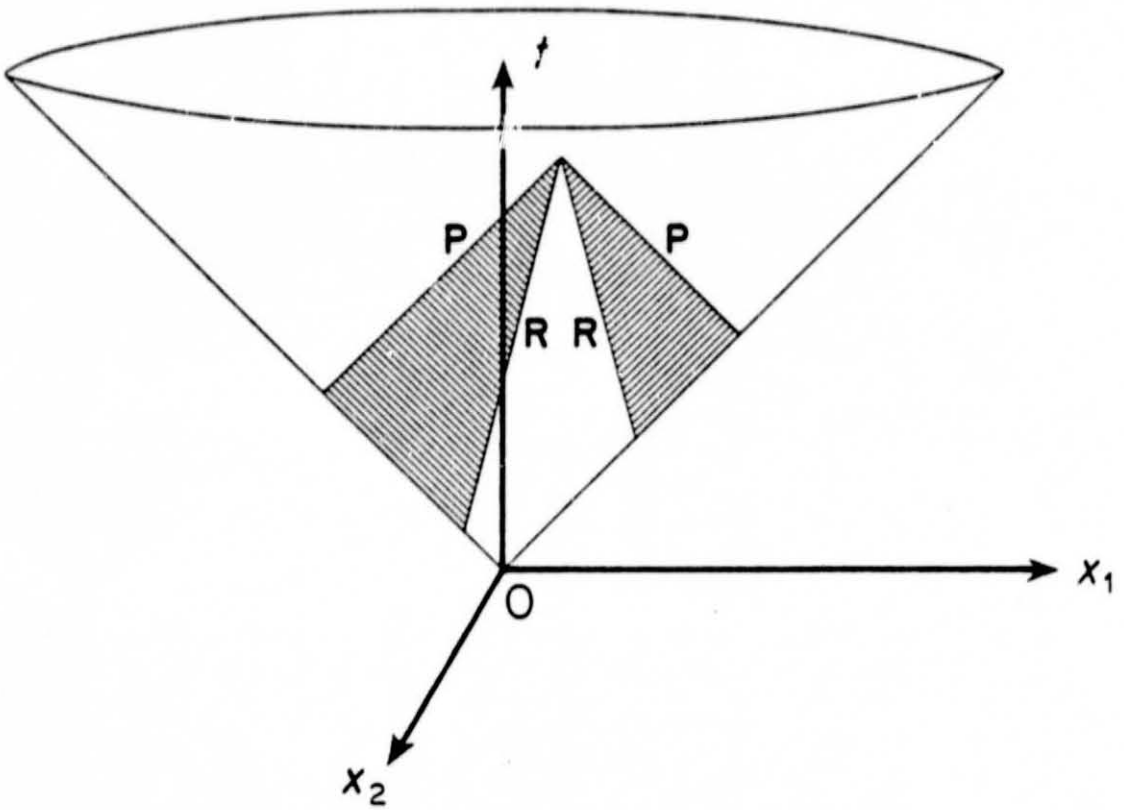

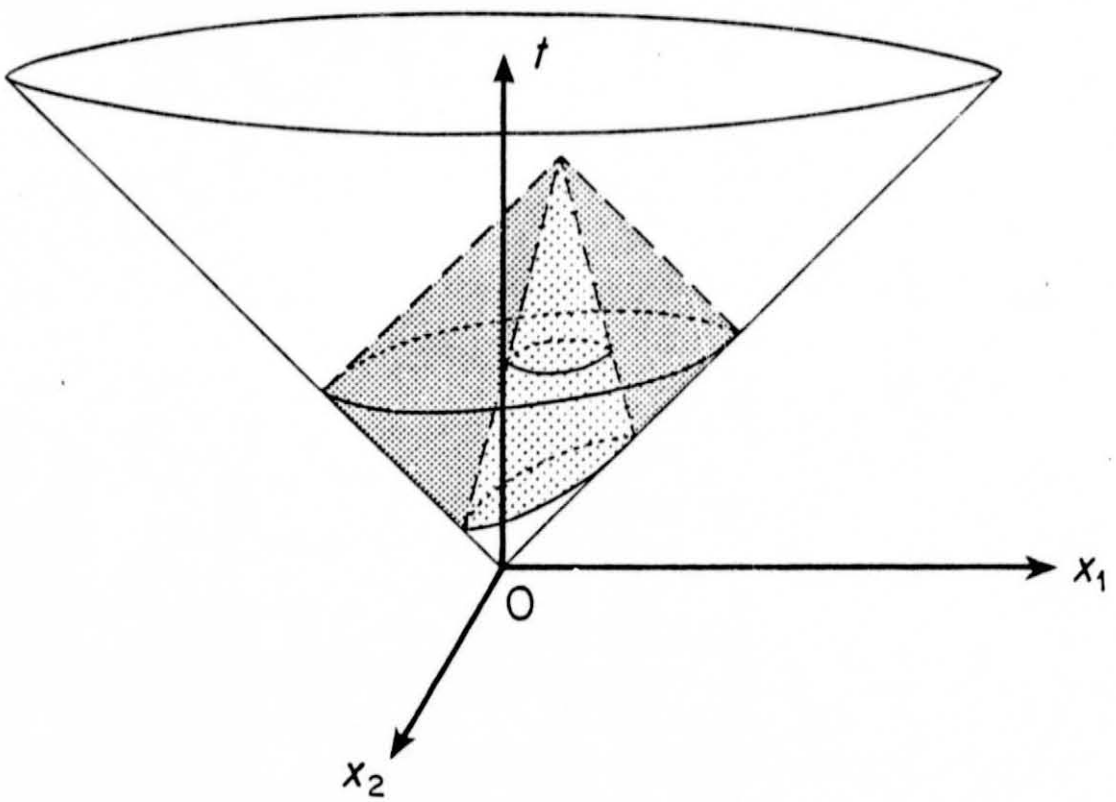

VOLUME OF INTEGRATION

Figure 2

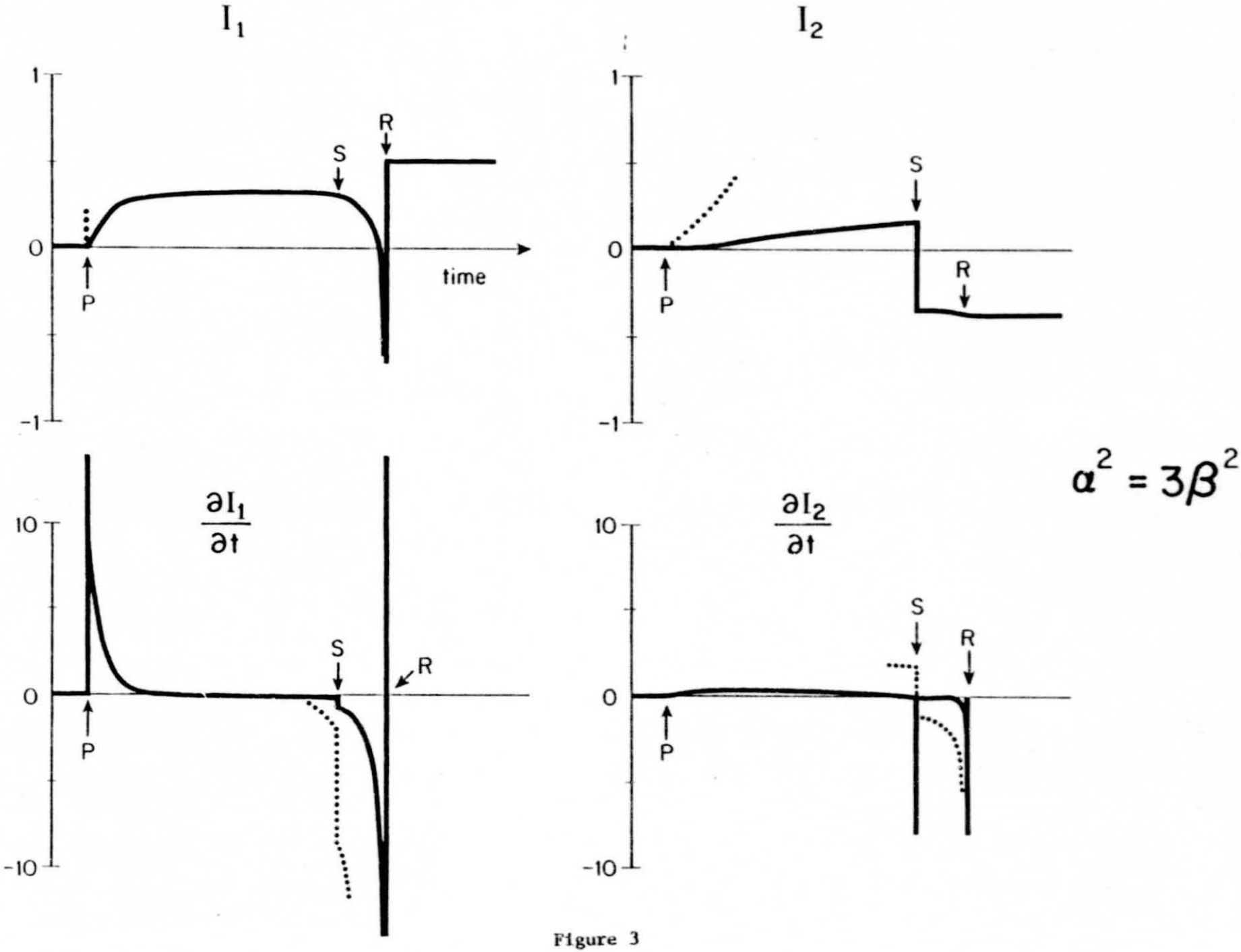
I_1
I_2
1
0
-1
R
S
P
time
$\frac{\partial I_1}{\partial t}$
$\frac{\partial I_2}{\partial t}$
10
-10
$\alpha^2 = 3\beta^2$

Figure 3

$F_{11}(X_1, X_2, 17.5)$

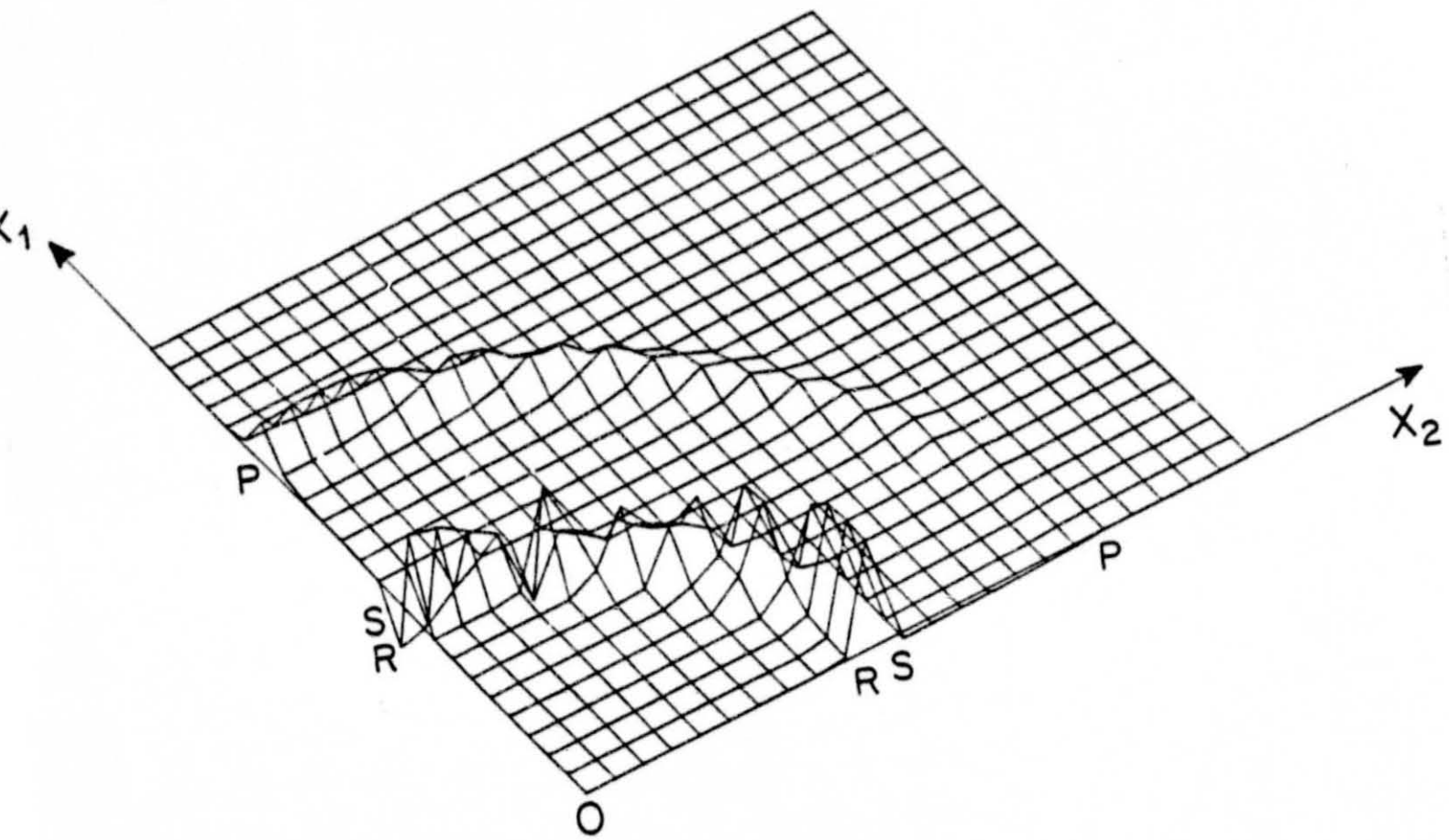

Figure 4

INSTANTANEOUS CIRCULAR PLANE SHEAR CRACK WHICH RADIATES WITHOUT GROWING

$$\alpha \frac{\Delta T}{\Delta X} = .5$$

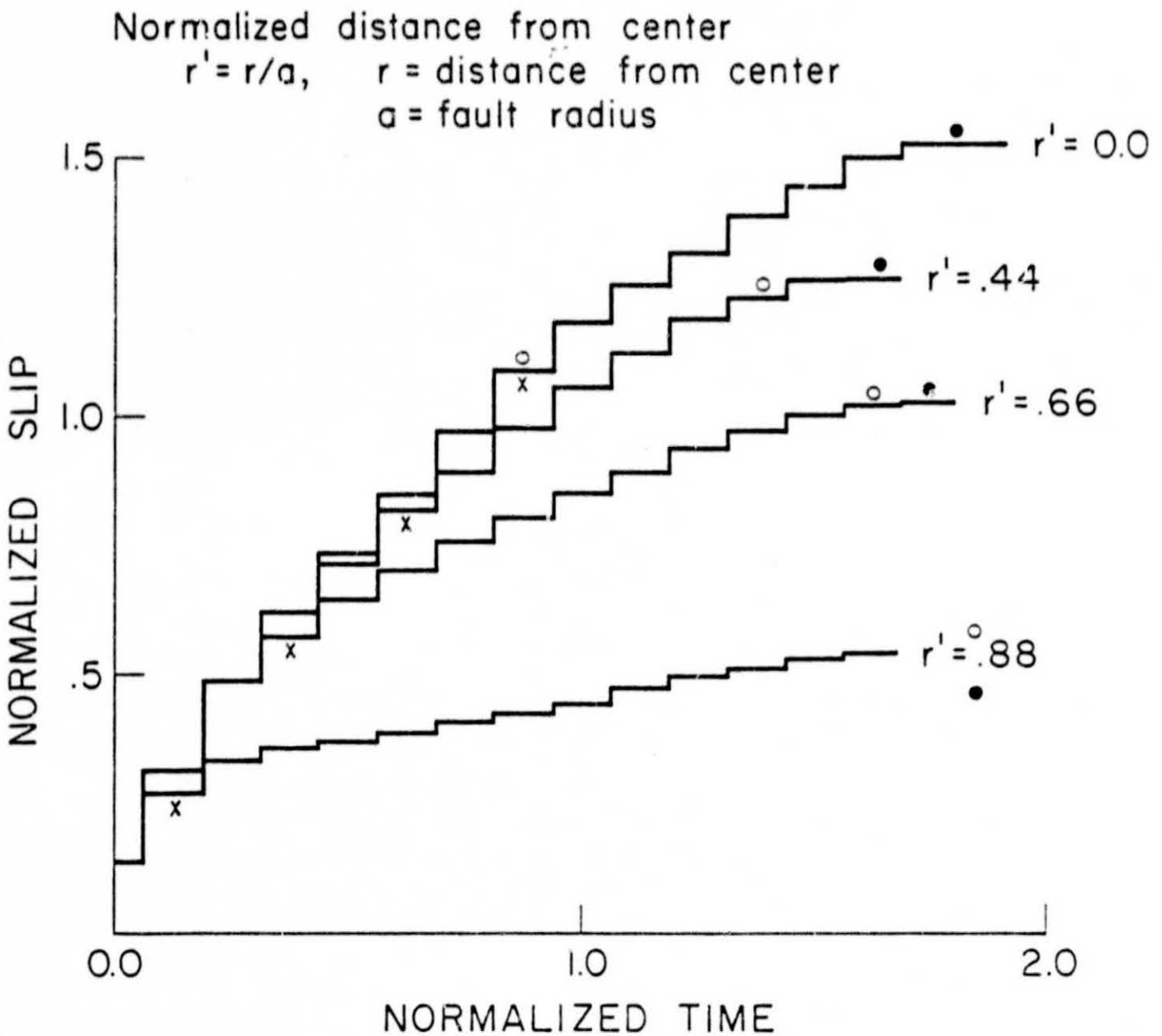

Figure 5

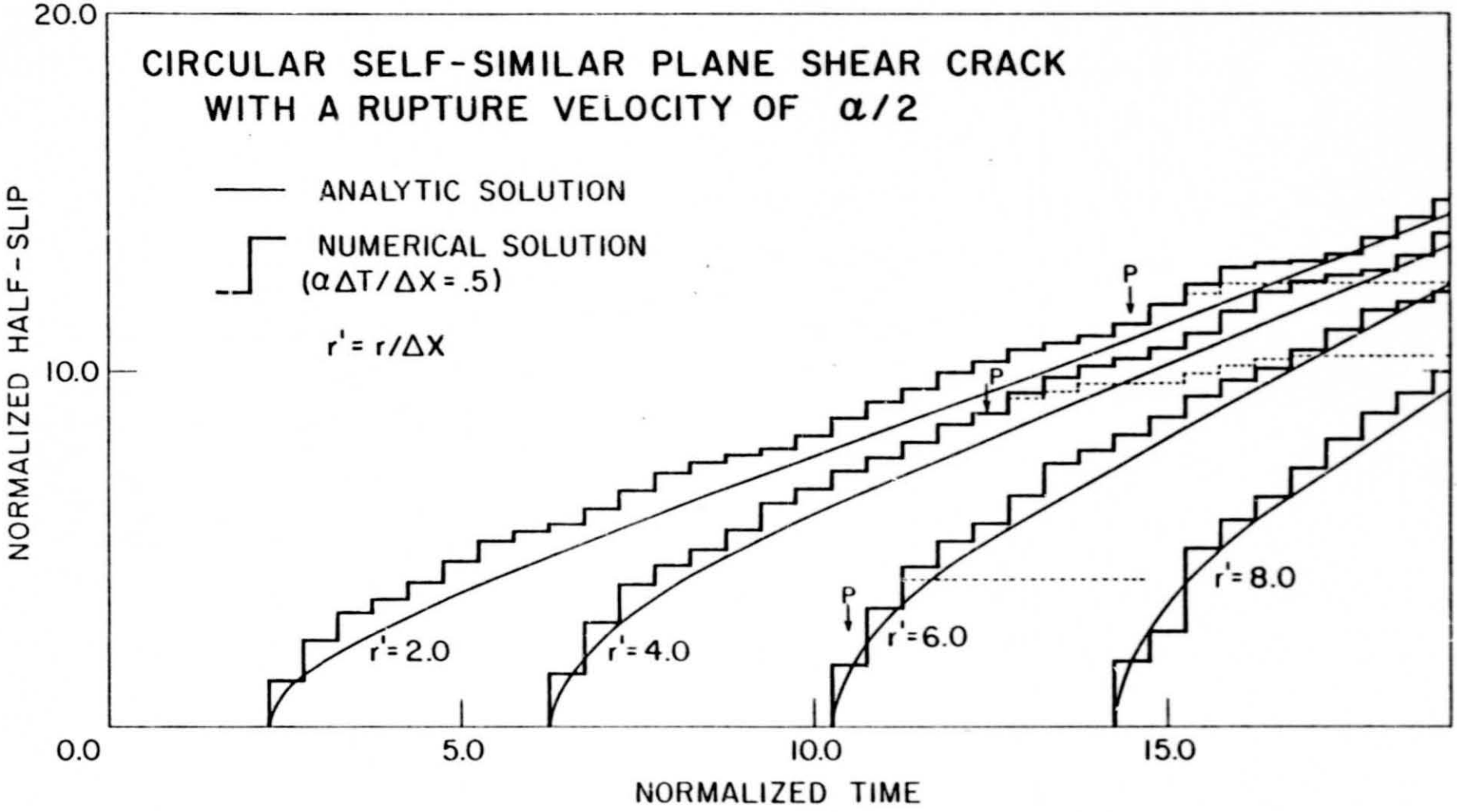
CIRCULAR SELF-SIMILAR PLANE SHEAR CRACK
WITH A RUPTURE VELOCITY OF α/2
ANALYTIC SOLUTION
NUMERICAL SOLUTION
(αΔT/ΔX = .5)
r' = r/ΔX
NORMALIZED HALF-SLIP
NORMALIZED TIME
20.0
10.0
0.0
5.0
10.0
15.0
P
P
P
r'=2.0
r'=4.0
r'=6.0
r'=8.0

Figure 6

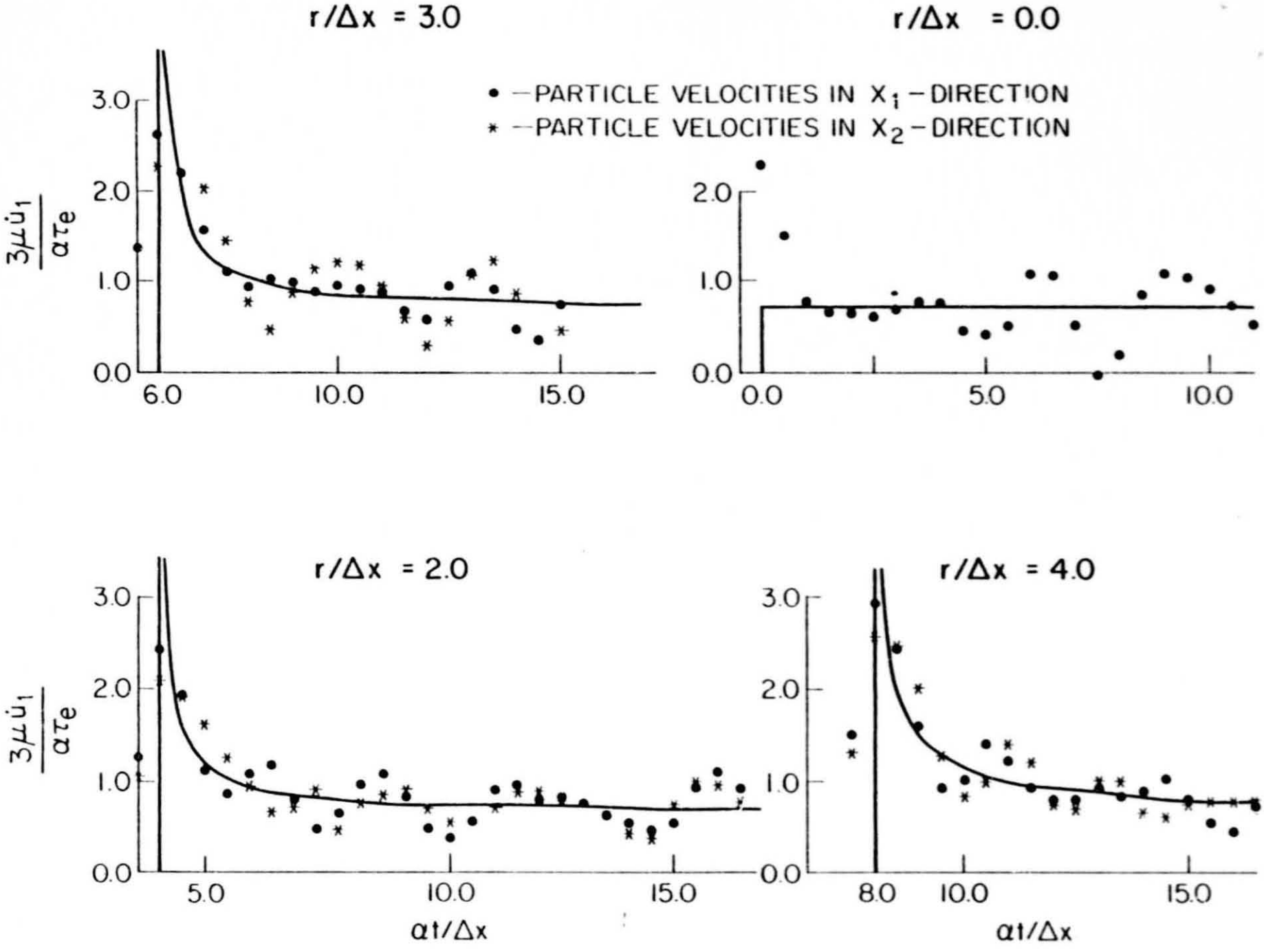
r/Δx = 3.0
r/Δx = 0.0
• —PARTICLE VELOCITIES IN X_1 – DIRECTION
* —PARTICLE VELOCITIES IN X_2 – DIRECTION
$\frac{3\mu\dot{u}_1}{\alpha\tau_e}$
3.0
2.0
1.0
0.0
6.0
10.0
15.0
2.0
1.0
0.0
0.0
5.0
10.0
r/Δx = 2.0
r/Δx = 4.0
3.0
2.0
1.0
0.0
5.0
10.0
15.0
αt/Δx
3.0
2.0
1.0
0.0
8.0
10.0
15.0
αt/Δx

Figure 7

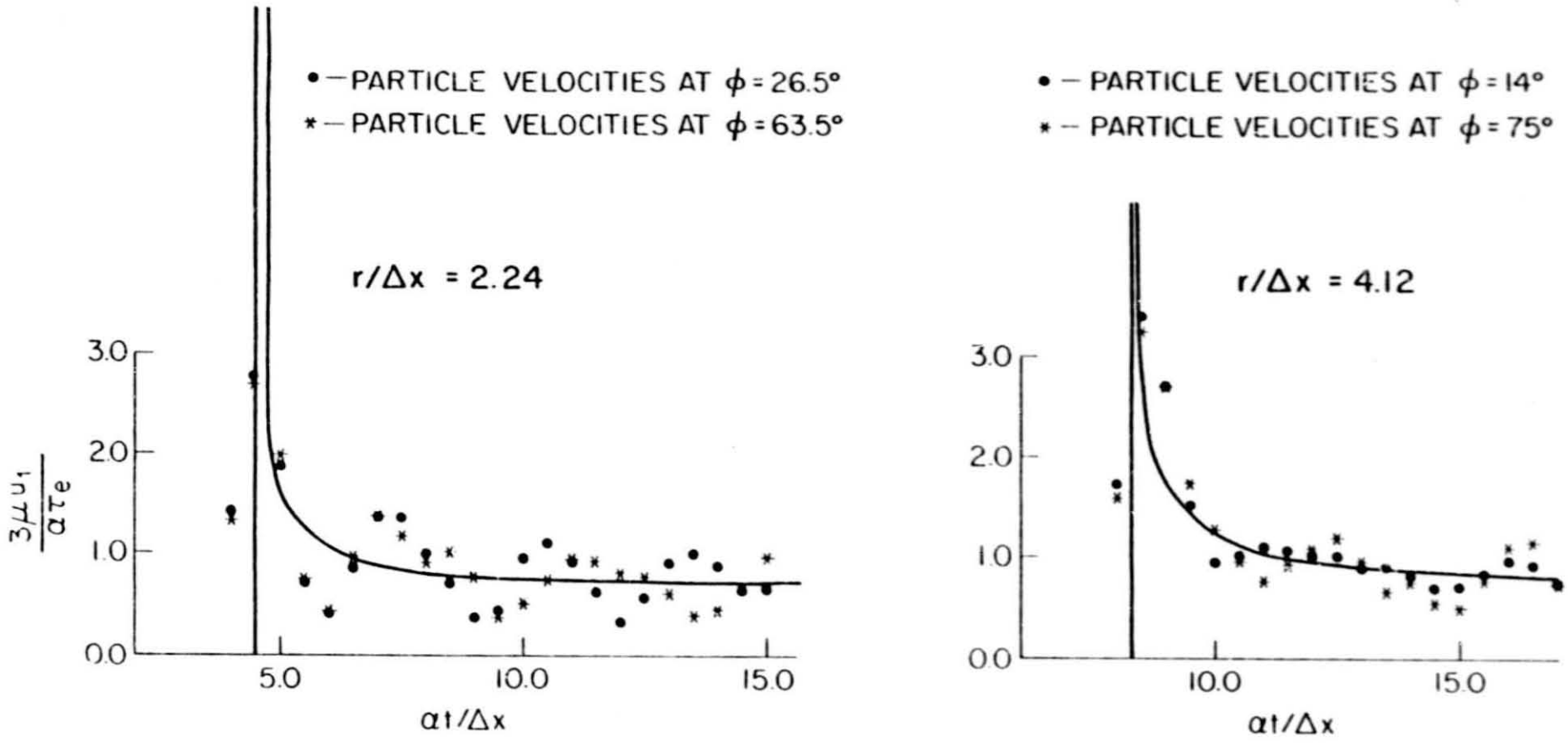
• — PARTICLE VELOCITIES AT $\phi = 26.5°$
* — PARTICLE VELOCITIES AT $\phi = 63.5°$
$r/\Delta x = 2.24$
$\frac{3\mu u_1}{\alpha \tau_e}$
3.0
2.0
1.0
0.0
5.0
10.0
15.0
$\alpha t/\Delta x$
• — PARTICLE VELOCITIES AT $\phi = 14°$
* — PARTICLE VELOCITIES AT $\phi = 75°$
$r/\Delta x = 4.12$
3.0
2.0
1.0
0.0
10.0
15.0
$\alpha t/\Delta x$

Figure 7